Published in final edited form as:
Microcirculation. 2011 April ; 18(3): 238–251. doi:10.1111/j.1549-8719.2011.00084.x.

Terminal arteriolar network structure/function and plasma cytokine levels in db/db and ob/ob mouse skeletal muscle

Melissa K Georgi[1], **Jacqueline Vigilance**[2], **Anthony M. Dewar**[1], and **Mary D. Frame**[1]
[1]Department of Biomedical Engineering, Stony Brook University, Stony Brook, New York, USA
[2]Faculty of Medical Sciences, University of the West Indies, Cave Hill, Barbados

Abstract

Objective—To investigate the terminal arteriolar network structure and function in relation to circulating plasma cytokine levels in db/db, ob/ob and their genetic background control, C57/bl6 mice.

Methods—Arteriolar network size and erythrocyte distribution were observed in the resting cremaster muscle (N=45, pentobarbital 50mg/kg i.p.). Structural remodeling and inflammatory state was related to 21 plasma cytokine levels.

Results—db/db networks were shorter, had fewer branches and smaller diameters than C57/bl6 controls. ob/ob networks were longer, with similar branch numbers yet non-uniform diameters. Shunting of erythrocytes to the specific terminal arteriolar branches of the network (functional rarefaction) was prominent in db/db and ob/ob, with further evidence of shunting between networks seen as no flow to 50% of ob/ob arteriolar networks.

Conclusions—Altered levels of plasma cytokines are consistent with structural remodeling seen in db/db, and a pro-inflammatory state for both db/db and ob/ob. Differences in network structure alone predict overall reduced uniform oxygen delivery in db/db or ob/ob. Shunting likely increases heterogeneous oxygen delivery and is strain dependent.

Keywords

inflammation; metabolic disorder; oxygen delivery; plasma cytokines

Introduction

Reduced oxygenation to peripheral tissues is associated with development of chronic ulcers and poor wound healing for patients with diabetic peripheral vascular disease (78). There are multiple structural and functional mechanisms to account for reduced tissue oxygenation. Oxygen delivery requires sufficient volumetric blood flow, but as a flow limited solute, oxygen delivery is a direct function of red blood cell flux, and hemoglobin saturation (8). In addition, architectural features, such as microvessel density and organization, will impact oxygen delivery by affecting the Krogh radius (39). In humans, diabetes and obesity are associated with structural rarefaction (decreased microvessel density) (18,24,56). The db/db and ob/ob mice are models of diabetes and obesity with the genetic modifications of absence of the satiety hormone leptin in ob/ob, and absence of the key leptin receptor (LRb−) in db/db (4,36); the C57/bl6 strain is the genomic background control for each. The db/db model

Corresponding Author: Mary D. Frame, Department of Biomedical Engineering, Bioengineering Building G19, Stony Brook University, Stony Brook, NY 11794-5281, Office: 631-632-1625, Fax: 631-632-3222, mframe@notes.cc.sunysb.edu.

displays structural rarefaction seen as a generalized loss of both capillaries and small arterioles (9,13,25). Corresponding information is missing from the literature for the ob/ob model, however, other rodent models of obesity show rarefaction (32,69). While structural rarefaction has been noted as a generalized decrease in microvessel density, the architectural organization of terminal microvascular networks has not been described for diabetic nor obese animal models. The primary purpose of our study was to examine microvascular network structure as an indicator of anatomic oxygen delivery capacity, in relation to circulating plasma cytokine levels for these models of metabolic disorder as compared to the C57/bl6.

The architecture of the terminal arteriolar networks was examined because the network provides the final active control of oxygen delivery to the level of the capillary (7,30,71). The branch arterioles arising from the central feed arteriole, directly empty into capillaries. We hypothesized that terminal arteriolar networks in db/db and ob/ob mice (compared to age-matched C57/bl6) would have decreased network size (length, number of branches, and diameters) as evidence for remodeling that suggests structural rarefaction. In addition, we hypothesized they would show functional rarefaction, seen as diminished red blood cell flux into the network, with non-uniform flux to the branch arterioles, consistent with spatial or temporal shunting. Lastly, we hypothesized that the db/db and ob/ob mice would show decreased plasma levels of proangiogenic cytokines, and increased levels of pro-inflammatory cytokines. This hypothesis is based on both the changes we observed in network structure, and the literature suggesting that metabolic disorder is both proinflammatory and associated with microvascular rarefaction.

Methods and Materials

Animal Preparation

All animal protocols were approved by the Institutional Animal Care and Use Committee of Stony Brook University. Three different strains of mice were used in these protocols: C57/bL6 (inbred, normal metabolism), ob/ob (obese, leptin deficient mice), or db/db (diabetic, leptin receptor deficient mice, LRb−). All mice were obtained from Harlan Laboratories (Somerville, NJ).

For architecture and erythrocyte flux observations, male mice (C57/bl6 n=34, db/db n=5, ob/ob n=6), were anesthetized with pentobarbital sodium (50 mg/kg, i.p.) and maintained on constant i.p. infusion to replace insensible fluid losses (volume flow of 0.1 mL/hr) and maintain an appropriate anesthetic plane (20mg Nembutal / kg / hr). Tracheostomy was performed to ensure a patent airway. Core temperature of the animal was maintained (37° – 38 °C) by conductive and convective heat sources. Respiratory rate and toe-pinch response were recorded each 15 minutes; mean arterial pressure was not monitored. Immediately post induction, blood samples were taken in triplicate via toe clip for blood glucose, plasma cytokine and systemic hematocrit measurements (50 μL per tube). In a second set of animals (C57/bl6 n=16, db/db n=12, ob/ob n=12) a blood sample was taken by toe clip immediately upon induction for blood glucose, plasma cytokine and hematocrit measurement. Blood glucose was measured using a clinical blood glucose meter (OneTouch Basic, LifeScan, Milpitas, CA). Systemic hematocrit was measured using a micro-hematocrit reader (Hemata Stat-II, Separation Technology Inc., Altamonte Springs, FL). Blood glucose and systemic hematocrit measurements were repeated from fresh blood samples (toe clip) at the end of the experimental day and compared to the initial values. Systemic hematocrit was determined at the start and end of these experiments as an indicator of the hydration state of the animals. The finding of no increase in hematocrit would confirm that the volume replacement rate (0.1 mL/hr) was sufficient to replace insensible fluid losses, e.g., due to respiration. Demographic information for these two groups of animals is shown in Table 1.

For architecture and erythrocyte flux observations (N=45), the right cremaster muscle was prepared for direct observation of the microvascular network, using the method of Baez (3). Briefly, after being freed from the scrotum, the cremaster muscle was incised longitudinally, separated from the testis and epididymis, including severing of the deferential feed vessels, cleared of connective tissue and gently extended over a glass pedestal by means of several insect pins secured in SylGard 34 (Dow Corning, Midland, MI). The testis and epididymis were gently placed into the abdominal cavity via the inguinal canal. The preparation was continuously superfused with bicarbonate-buffered physiological salt solution (control suffusate) containing (in mmol) 132 NaCl, 4.7 KCl, 2.0 $CaCl_2$, 1.2 $MgSO_4$, and 20 $NaHCO_3$ (equilibrated with 5% CO_2−95% N_2 gas, pH 7.4 at 34°C). All chemicals were obtained from Sigma Chemical (St. Louis, MO), unless otherwise noted.

Fluorescent labeling of RBCs for use as flow markers

Red blood cells (RBCs) were fluorescently labeled using a modified method after Sarelius (63). Mice (male C57/bl6 27.3±2.7 gm, 105.6±22 days, N=36) were anesthetized with pentobarbital sodium (50 mg/kg). Blood collection was performed via a heart puncture into heparinized tubes (standard 7ml green top, Becton-Dickinson), centrifuged (2000 rpm, 5 min), and the plasma and buffy coat removed. Residual red blood cells were washed with HEPES buffered physiological salt solution (HBS, pH 7.4), centrifuged, and the HBS supernatant aspirated. Remaining red blood cells were mixed with 0.05 μg substituted tetramethyl rhodamine isothiocyanate (XRITC, Molecular Probes, Eugene OR) first dissolved in 60 μL DMSO and then combined with 25 mL HBS (pH 8.1) and incubated at room temperature for 1 hour. These RBCs were washed seven times using HBS (pH 8.1) with bovine serum albumin (BSA, 0.5g%), stored at 4°C in HBS (pH 8.1) with BSA (0.5g %), and used within three days. Approximately 0.05 mL of 50% packed RBCs in saline was injected into the right jugular catheter 30 minutes prior to data acquisition. Due to the difference in animal weight, total volume injected into the animals was approximately 4% of the total blood volume of a C57/bl6 mouse or 2% of an ob/ob or db/db mouse, using the weight to estimate blood volume (16).

Experimental Protocol

The microcirculation was observed with transillumination using a modified Nikon upright microscope (Nikon, Tokyo, Japan), using a 25× objective (Leitz, NA 0.35), and secondary magnification of 1.5× (total optical magnification 37.5×) or with a 60× salt water immersion objective (Nikon, NA 0.90) and no secondary magnification. Video images were produced by using an intensified charge-coupled device (ICCD) video camera (Solamere Technologies Group, INC., XR/ABF, Palo Alto, CA) and video recorded (Panasonic SVHS AG7350).

During a 60 minute stabilization period, arteriolar tone was verified by confirming dilation to topically applied 10^{-4} M adenosine (ADO, used to obtain maximal diameters) and constriction to topically applied 10^{-4} M phenylephrine (PE, used to obtain minimum diameters). Tone ([peak diameter-baseline diameter]/baseline) was equivalent in each strain; for the entrance to the feed arteriole the ADO response was: C57/bl6, 0.20±0.12; db/db, 0.14±0.11; ob/ob, 0.22±0.15; and the PE response was: C57/bl6, −0.23±0.15; db/db, −0.13±0.14; ob/ob, −0.14±0.12 (mean±SD). At least 30 minutes was allowed after adenosine and phenylephrine application before obtaining architecture and flux data.

All observations were made at defined locations along terminal arteriolar networks, shown schematically in Figure 1. These networks were functionally defined using the description of Sweeney and Sarelius for the hamster microcirculation (72). While the networks were identified in the presence of adenosine to ensure that all anatomic branches were located, the

functional data (flow) and associated architectural data (diameters and lengths) were videorecorded at least 30 minutes after adenosine and phenylephrine application. Observations were made at the entrance to the network, as the feed arose from the arcading arteriole, and then at sequential branch points to the last branch, where both arterioles terminated in only capillaries. In the single instance (in one db/db) that only a single arteriolar bifurcation was present; it was designated as 'last'. Sequential branch points were videotaped for 30 seconds each, taking not more than 5 minutes to record a whole network. A combination of brightfield and epifluorescence (Chroma G1A, Chroma Technology Corp.) was used to obtain diameters and fluorescent cell flux simultaneously.

Architectural Measurements

Four different architectural measurements were obtained from each network: total network length, inter-branch length, diameters, and number of bifurcations. Total network length and inter-branch length were measured off-line directly from the video image using a flexible ruler to follow the normal contours, and was calibrated using a micrometer, shown schematically in Figure 1. To measure diameters, video images were converted to bmp format (XCAP, Epix Inc, Buffalo Grove IL). The internal diameters were measured for the feed before the branch, and the branch, within 1 tube diameter of center of mass of the bifurcation (ImageJ, NIH).

Erythrocyte Flux Measurements

Video images were converted to uncompressed AVI 1.0 files (XCAP, Epix Inc, Buffalo Grove IL). Erythrocyte (red blood cell, RBC) flux was measured as the number of fluorescently labeled cells entering a bifurcation during a 30 second time period. The flux to the branch and feed continuation segments was noted. The cell fraction of fluorescently labeled cells within the total red blood cell population was determined at the end of the experiment by sampling the blood (toe clip), and making a dilute blood smear on a glass slide. This slide was videotaped at 10 locations using brightfield light (to identify total cells) and epifluorescence (to identify fluorescent cells). Off-line, each video image was examined, counting the fluorescent cells and total cells to provide the cell fraction, p; the average value of p was 0.0313±0.0547 (mean±SD, N=45). Cell flux, F cells/sec, is given by $F = m / p$, where m is the number of fluorescent cells observed in vivo, and p is the fluorescent cell fraction.

Plasma cytokine measurements

Whole blood from the post-induction toe clip was immediately centrifuged and the plasma was collected. Blood plasma was stored at −20°C for not longer than 6 months. Blood samples for cytokine measurement were pooled within strains to get the required volume of 0.5 mL for testing. Thawed plasma was pooled by mouse strain (2–4 animals per determination), and diluted in standard serum diluent to previously determined optimal incubation conditions. Plasma cytokines were measured (Beadlyte Mouse 21-Plex Cytokine Detection System, Upstate Cell Signaling Solutions, Lake Placid, NY) using a Bio-Plex 200 System (Bio-Rad, Hercules, California) available as a core facility.

Statistical Analysis

All data are presented as mean±SEM. Student's paired t-test and one-way analysis of variance (ANOVA) with Tukey's post-test were used in analysis. RBC flux data at each bifurcation was normalized to the flux at the entrance to the network immediately downstream of the arcade. Populations were considered significantly different when $p < 0.05$. Variability was analyzed by the coefficient of variation (CV=SD/mean); the ratio of CV for the test group to the CV for the age-matched C57/bl6 mice (Table 3) is less than

unity when the test group is less variable than the control group, and greater than unity when the test group is more variable than the control group. (65)

Results

Murine demographics

Demographic statistics for the three strains of animals are shown in Table 1. Both metabolic disease strains are bred to express their respective disease phenotypes early in the course of their lifespan, with the db/db phenotype beginning to revert to normal at 14 weeks of age (35). We chose to perform our experiments at the peak of the phenotype expression in the metabolic strains, and provide two groups of C57/bl6 for comparison: age-matched and older mice.

As expected (52,59), the db/db and ob/ob mice were heavier than the metabolically normal genetic background control animals, C57/bl6 (Table 1). The older C57/bl6 mice were also heavier than the younger age-matched C57/bl6 mice. Baseline non-fasting blood glucose was higher in both db/db and ob/ob compared to the age-matched mice, and was significantly less (yet still within the normal range of 60 – 175 mg/dl (19)) in the older mice for only the plasma cytokine group (Table 1). The acute experimental procedures lasted 334±74 minutes (mean±SD) for the architecture and flux group, and 327±94 minutes for the plasma cytokine group, and were not different by age or strain. Both groups of C57/bl6 mice showed lower blood glucose levels, as expected for a normal fasting mouse. However, both the ob/ob and db/db animals continued to show elevated blood glucose levels post-protocol.

Post-induction hematocrit values were compared to those post-protocol to verify that the mice were appropriately hydrated while anesthetized (see Methods). The C57/bl6 strain had a significantly lower hematocrit post-protocol in both groups of animals, suggesting these animals may have been dehydrated upon induction. Also post-protocol, the db/db mice in the architecture and flux data group had an elevated hematocrit compared to the C57/bl6 mice, but this value was not elevated compared to the post-induction values for these same animals. Otherwise, hematocrit did not differ across strains for post induction nor for post protocol.

Network Structure

Total network length and number of branches are shown in Table 2. Diabetic (db/db) mice had shorter networks and fewer branches per network than all other groups. The ob/ob mice tended towards longer networks than the C57/bl6, but due to the variability in the ob/ob network lengths, this was not significant ($p=0.24$). In order to determine if changes in distance were equally distributed along the network, inter-branch lengths (the distances between branches) were measured (Figure 2). Inter-branch lengths did not differ along networks for any strain. Across strains, the the distance from the 2nd to the 3rd branches was longer for the ob/ob mice compared to the others. Additionally, the variability, especially in the ob/ob mice, was high, as seen by the very high standard deviations. Examining the coefficient of variation for each strain, the variability in the total length was 32–35% lower in either the db/db or the older C57/bl6 as compared to the younger C57/bl6 mice, while this variability was 54% greater in the ob/ob mice compared to the younger age-matched controls. Variability in the interbranch distances for db/db mice was likewise less than the age-matched C57/bl6 mice (Table 3); in contrast, the variability in inter-branch distances for the ob/ob mice was branch dependent with the highest variability (>50%) at the 1st bifurcation. The older C57/bl6 animals followed the trends for the ob/ob mice. Thus, db/db networks were uniformly shorter with more evenly spaced branches compared to C57/bl6. In

contrast, ob/ob networks were highly variable in total length, with non-uniform spacing of terminal branches along the length.

Internal resting diameters were measured for the feed arteriole (Figure 3) and each branch (Figure 4) at sequential bifurcations for the 1st, 2nd, 3rd, and last arteriolar branch points. Diameters for the feed and branch in the db/db networks were smaller at the first bifurcation compared to other groups. For both the feed and branches at all other locations, there were no differences in diameter between the groups. The feed diameters were less variable for the db/db, and in general, more variable for the ob/ob or older mice compared to age-matched C57/bl6 mice, but again bifurcation dependent (Table 3). Thus, in the db/db networks the feed diameter was uniformly smaller than in the other groups, while the networks from the ob/ob or older mice were more variable upstream, specifically at the entrance to the network vs. C57/bl6. Branch diameters were instead more variable at all branches in the db/db and ob/ob mice vs. the age-matched C57/bl6 mice, and at the 1st and 3rd branches for the older mice. Thus, there is evidence for structural remodeling for both the db/db mice (diminished network length with decreased luminal diameters) and the ob/ob mice (similar branch numbers with irregular-sized diameters spaced along a longer central feed). In either case, the networks suggest an apparent sparse filling of the tissue area that occurs differently in the db/db vs. ob/ob networks.

Network erythrocyte flux

Two factors are important in comparing total influx of cells to each network: the fraction of networks without measurable erythrocyte flux over 30 seconds; and the variability in the total influx for those networks with flow. Out of 29 networks in the age-matched C57/bl6 mice, 42% had no flux; of 5 older C57/bl6 mice, only 20% had no flux; of 5 db/db mice, 40% had no flux; of 6 ob/ob mice, 50% had no flux. The average baseline erythrocyte influx to networks with flow is as follows: C57/bl6 networks had 134±90 cells/second (mean±SD); older C57/bl6 networks had 85±67 cells/second; db/db networks had 44±19 cells/second* ($p<0.05$ vs age-matched C57/bl6); ob/ob networks had 63±34 cells/second. Variability (coefficient of variation) in the total influx was 57% more for the older mice, 26% less for db/db mice and 8% less for the ob/ob each as compared to the age-matched C57/bl6 mice. Thus, there is evidence of functional rarefaction across networks in the db/db seen as decreased influx per network, while all of the age-matched mice showed similar fractions of networks with negligible flow.

Erythrocyte distribution within the networks was determined as an indicator of altered oxygen delivery (or altered Krogh cylinder radius) to specific locations (terminal branches) within the networks. Raw erythrocyte flux (cells/second) and fractional flux to each branch is shown in Figure 5. In C57/bl6 mice, successive branches received fewer erythrocytes, with the 3rd and last branches receiving significantly less than the 1st branch, and 35% of the inflow passing to the anatomically larger of the last branches, designated as the Last Feed. This Last-Feed vessel received more erythrocytes than did the 2nd, 3rd, or last branches. This trend was significant when examining the raw cells/second, and was mirrored when looking at the fractional influx distribution (Figure 5, A vs. B). Thus in the control strain, over half of the erythrocyte flux was distributed to the branch arterioles (nutrient flow), while 35% was shunted through the network. This pattern was not seen in the older C57 mice, with most inflow (45%) passing to the 1st branch, and the Last Feed receiving fewer cells than the other groups.

For db/db mice, the 1st and last branches received a similar fraction of the inflow compared to the age-matched C57/bl6 mice, but the total number of cells was significantly less, with 73% of the total influx passing to the Last-Feed. For the ob/ob mice, the 1st and 2nd branches received a similar fraction of the total inflow compared to the age-matched C57/bl6 mice,

but this was significantly fewer total cells to the 1st branch. The 3rd and last branches for the ob/ob group received significantly fewer cells than the upstream branches with most of the erythrocyte flux (58%) being shunted to the Last-Feed vessel. Thus for both the db/db and ob/ob, evidence of functional rarefaction was seen as increased shunting of erythrocytes to the Last-Feed, to the extent that cells were stolen from some of the upstream branches. While the fractional flux to the 1st branch was maintained, the total number of cells was significantly less. Functional rarefaction within the network was additionally seen for the ob/ob mice as a disparity in RBC flux distribution with upstream branches receiving more RBC flux than the 3rd and smaller last branches.

The variability in erythrocyte flux (Table 3) showed that the raw flux in cells/second for both db/db and ob/ob was less than or as variable as flux for the age-matched C57/bl6 at all branches except the 2nd (ob/ob), while the fractional influx was more variable to the branches, for these strains. The Last Feed vessel was instead more variable for the ob/ob than the db/db mice. The older C57 mice instead showed a flux distribution that was as variable as the younger C57, but the raw flux distribution was much more variable.

Plasma cytokine levels

Structural remodeling for the db/db mice (diminished network length with decreased luminal diameters) and the ob/ob mice (similar branch numbers along a longer central feed) suggests very different angiogenic changes for these two strains. To provide insight into potential systemic mechanisms involved in the structural remodeling, we measured the plasma levels of 21 cytokines for these murine models; these blood samples were taken immediately upon induction of anesthesia. The results are shown in Table 4. First, the older vs younger C57/bl6 mice showed very few significant differences in cytokine levels: the anti-inflammatory IL-9 and IL-13 levels were significantly higher in the older mice. Otherwise, there were no significant differences between these age groups. The db/db population had higher levels than the age-matched C57/bl6 mice for IL-1alpha and KC, with lower levels for IL-1beta, IL-2, IL-3, IL-4, IL-5, IL-9, IL-10, IL-12, IL-13, GM-CSF and IFNgamma. The ob/ob population had higher levels than the age-matched C57/bl6 mice for IL-1alpha, IL-1beta, IL-2, IL-5, IL-13, KC, RANTES and VEGF, with a highly variable MIP-1beta level. Cytokines with lower levels in the ob/ob than those of the age-matched C57/bl6 mice include IL-3, IL-9 and GM-CSF. Additionally, several cytokines differed between the db/db and ob/ob populations, including IL-4, IL-5, IL-10, IL-12, IL-13, IL-17, GM-CSF, IFNgamma, RANTES and VEGF. Finally, there were significant differences between the older C57/bl6 population and the db/db or ob/ob, some, but not all, following the trend as for the age-matched group, noted in Table 4, but their significance is not considered further.

Discussion

This study provides novel data regarding the peripheral microvascular phenotypes and circulating cytokines levels for db/db and ob/ob mice. Structural remodeling suggestive of rarefaction, is seen for both the db/db mice (diminished network length with decreased luminal diameters) and the ob/ob mice (similar branch numbers along a long central feed with irregular branch size), as compared to age-matched C57/bl6 mice. Functional rarefaction is seen within networks in the db/db or ob/ob mice, as increased shunting of erythrocytes through the network and unequal flux distribution to each branch. Shunting in this sense could also be interpreted as a situation where a larger Krogh radius is required to maintain oxygen delivery due to the decreased numbers of flow paths. Further, across the networks for the age-matched C57/bl6, db/db and ob/ob mice, functional rarefaction is seen as 40–50% of networks without perceptible erythrocyte flux, unlike the older C57/bl6 mice for which only 20% of networks had no flow. Lastly, there are clear indications that the

structural remodeling in db/db networks is associated with decreased plasma pro-angiogenic cytokine levels.

Peripheral microvascular networks in db/db and ob/ob models

In humans, diabetes and obesity are associated with structural rarefaction (decreased microvessel density) (18,24,56). In the present study, we examine the microcirculation of db/db and ob/ob mice as models of diabetes and obesity, respectively. Rarefaction in rodent models of obesity appears to be common (32,69); the present study is the first to report structural rarefaction in ob/ob mice. Generalized structural rarefaction of capillaries and small arterioles is documented for the db/db mice (9,13,25), yet the relationship to oxygen delivery flow paths was not clear in those studies. In the present study we examined changes in terminal arteriolar network structure and function to indicate remodeling in the db/db and ob/ob mice. Terminal networks are the distal most location of active control of blood flow to the level of the capillary (7,30,71). This is a different measure than examining a generalized capillary or arteriolar density, but is a measure of alterations in potential control of oxygen delivery to the level of the capillary.

We hypothesized that both the db/db and ob/ob networks would be shorter and with fewer terminal branch arterioles than the C57/bl6 mice. Instead, two distinct phenotypes of structural remodeling were found: db/db networks are significantly shorter with fewer branches and decreased luminal diameter, while the ob/ob networks are significantly longer on average, yet have comparable branch numbers as compared to their background genetic control, C57/bl6 mice (Table 2). Considering that resistance to flow is proportional to the length of a tube, and inversely proportional to the fourth power of the radius, our data suggests that resistance is elevated within terminal arteriolar networks for both db/db and ob/ob mice. Reducing the resistance term of the Hagen-Poiseuille equation ($R = 8 * \text{viscosity} * \text{length} / \pi * \text{radius}^4$) to length divided by the 4^{th} power of the radius, the estimated resistance along the central feed arteriole is increased 2.2 times for the db/db or the ob/ob, compared to the age-matched C57/bl6 mice. The older population of C57/bl6 mice instead showed only a 50% increased resistance. Thus, the structural differences seen in both metabolic models will potentially affect convective flow of blood to the terminal branches of the networks, and possibly also oxygen delivery, yet though through different structural features. While intravascular pressures were not measured here, this argument suggests that the pressure gradient along these networks would need to be increased 2.2 times in the metabolic models to maintain mass flow along these networks. Evidence suggests that mass flow was not maintained for the db/db nor ob/ob networks. Instead, using erythrocyte flux to indicate flow, the db/db mice displayed 25% of the influx of the age-matched C57/bl6, and the ob/ob displayed a highly variable 50% of the influx of the controls. A notable caveat is that the Baez method (3) for preparing the cremaster muscle requires severing of the deferential arteries, which results in decreased inflow pressures to the cremaster and has been shown to alter tone in these larger arterioles (34,51), but it is unclear what effect this has on flow into the terminal networks. For a complex network of flow in series and in parallel, total inflow to individual networks may be diminished, the numbers of perfused networks may be decreased, or the impact may be minimal at this level. As all preparations here used the Baez method, and there were clear differences between the groups regarding numbers of perfused networks, total influx and flux distribution, we limit our interpretation to comparisons between our experimental groups and do not speculate regarding the model itself.

Each phenotype suggests that there is increased heterogeneity of oxygen delivery (measured as erythrocyte flux, Figure 5) due to structural and functional differences in the db/db and ob/ob networks compared to the age-matched C57/bl6. Regarding capillarity, although decreased capillary density is reported for the db/db mouse (9,25), it is unknown whether the

size of the capillary groupings (modules) fed by each branch is uniformly decreased for each branch, or whether there is a decreased capillary density occurring preferentially for those capillaries fed by low-flow branches. The latter notion would be consistent with the well known flow induced pro-angiogenic process (48), and the absence of flow being an early signal for apoptosis (75). Here, we would hypothesize that capillary density preferentially decreases in areas that are poorly perfused. We showed evidence of functional rarefaction (shunting) of RBCs that is also consistent with increased heterogeneity of oxygen delivery within the networks. Shunting of ~50% of the influx to the larger last branch was common for the ob/ob mice. For the db/db mice, the network influx was statistically less than influx for the C57/bl6 or ob/ob. Despite that the 1st branch in db/db mice received a similar fraction of the influx as did the 1st branch in the C57/bl6 or ob/ob, the total flux (cells/s) to that 1st branch was much less for the db/db. Lastly, db/db showed that a striking 73% of the influx was diverted to the anatomically larger last branch, yet this was still statistically fewer cells (hence less oxygen) than the larger last branch received in the other models. We have reported shunting of RBCs of this magnitude to the anatomically larger last branch of networks in a hamster model of systemic inflammation (50), and thus this may be a common feature in peripheral inflammation. Shunting within the ob/ob networks was also seen with the 1st and 2nd branches receiving significantly more flow than the 3rd or last (anatomically smaller) branches. Together this suggests heterogeneity of oxygen delivery within the networks that is exaggerated in db/db and in ob/ob mice. Further, the ob/ob mice displayed 50% of networks having no flow, suggesting a broad heterogeneity of oxygen delivery across the tissue. This indicates that half of the flow through this tissue, in both the metabolically normal and metabolically altered animals, is likely to be non-nutritive (or the Krogh cylinder must be larger), and for the db/db and ob/ob further suggests that a large part of the tissue is underperfused. Remaining to be determined is the actual size of the capillary bed fed by each branch.

Angiogenic cytokines in diabetes and obesity

Examining the literature, most of the cytokines we report are not found for the db/db or ob/ob mice, and levels reported for these mouse models are age dependent, as expected, since the models develop diabetes or obesity over time, and then revert to a metabolically normal phenotype after 14 weeks of age (67). For instance, despite that IL-6 production is elevated in isolated aortic endothelial cells harvested from db/db mice (unknown age) (68), plasma IL-6 levels are not different from controls in 70 day old db/db (33), and are significantly decreased in 168 day old db/db (55). Our data show IL-6 to be significantly decreased in 80-90 day old db/db. KC levels (mouse ortholog of IL-8) were increased in 84 day db/db mice (26,68), similar to our findings. IL-10 levels were found to be normal at 14 days, and elevated by 70 days in db/db mice (14), while we report they are decreased significantly in 80–90 day old db/db. TNFalpha levels are similar in db/db and control mice at 70 days (33); we report they are also similar. For ob/ob mice, plasma levels for several cytokines are reported. IL-17 is decreased in ob/ob mice over 112 days (58); we report no change from control in our 75–80 days old ob/ob. IFN-gamma is unchanged is ob/ob at 115 days (58), but is significantly decreased at 210 days (47); we report no change from control. VEGF is not different from control in normal chow fed ob/ob mice (168 days (31)); we report a significant increase. IL-5 is decreased in 210 day ob/ob mice (47); we report no change from control. IL-6 levels in ob/ob mice are double control at 119 days (23), and then significantly reduced by 210 days (47); we report IL-6 to be 40% greater than that of control by 75–80 days. IL-10 in ob/ob mice is significantly decreased by 112 days (23), and 210 days (47); we report no difference from controls. Thus, insufficient information is found in the literature to interpret our findings in light of the animal phenotypes and range of ages reported.

The altered cytokine levels in db/db and ob/ob murine models do not follow levels of circulating cytokines found uniformly in diabetic/obese humans, nor in other animal models. For instance, other models of diabetes show increases in IL-1beta, GM-CSF, TNF-alpha and IL-12 (49,62,64,67,76,81), while we show that these factors are decreased in db/db mice. MIP-1b and RANTES are decreased in obesity (70), yet are increased in ob/ob mice. IL-3 is increased in human diabetics (42), yet decreased in both ob/ob and db/db mice. Thus a direct comparison of our findings to human or other models of diabetes or obesity is not appropriate. Given these limitations, we have examined how the changes in microvascular architecture for these genetically modified mice were related to plasma levels of pro-angiogenic and pro-inflammatory cytokines.

Of interest to us is the variability in network structure seen for these two models. While db/db networks were uniformly smaller in length and in diameter with evenly spaced branches, the ob/ob networks were highly variable in total length and in branch diameter, yet retained uniform spacing of terminal branches along the length. It is these architectural features that we examined in relation to circulating plasma cytokine levels. Of the 21 cytokines we measured, 12 are linked to pro-angiogenic actions and 3 are linked to anti-angiogenic actions. Pro-angiogenic cytokines are: IL1alpha, IL-1beta, IL-17, GM-CSF, TNFalpha, MCP-1, MIP-1b, VEGF, IL-3, IL-4, IL-6 and IL-13 (2,10–12,15,20,27,37,40,43,57,66,73,74,79). Anti-angiogenic cytokines are: IFNgamma, RANTES and IL-2 (1,5,74).

For the db/db mice, eight pro-angiogenic cytokines were significantly decreased, three were unchanged, TNFalpha (induces endothelial tube formation, M5), MIP-1b and MCP-1 (mural cell recruitment, (2), and one was elevated, IL-1alpha. Thus, eight pro-angiogenic cytokines are reduced in db/db mice; Importantly, VEGF was decreased, which is of course, essential for angiogenesis (26,68). Further, patterns of cytokine levels suggesting a suppression of angiogenesis are seen for the db/db mice, with a decrease in IL-1beta (stimulates IL-6, (40)), decrease in IL-6 (increases vascular smooth muscle production, (37), and enhances VEGF production (17)), and a decrease in GM-CSF (stimulates VEGF production, (15); stimulates IL-6 and MCP-1, (27)). Yet, two anti-angiogenic cytokines were decreased in the db/db mice (IFNgamma, IL-2). Thus, the plasma cytokine levels for the db/db mice indicate that angiogenesis (vascular remodeling) would be impaired in the db/db mice, and are consistent with an overall decreased network size (present study), and decreased capillarity and numbers of small arterioles in general (9,13,25).

For the ob/ob mice, the story is less clear. Several pro-angiogenic cytokines were elevated: IL-1alpha, IL-1beta, VEGF, and IL-13. This may be related to the increased length of the central feed in ob/ob networks. Other pro-angiogenic cytokines were decreased: GM-CSF (stimulates IL-6 and VEGF, (15,27)) and IL-3 (stimulates endothelial cell tube formation, (20)). Further, anti-angiogenic cytokines were elevated: RANTES and IL-2. Lastly, the absence of leptin itself must be considered. Leptin, absent in the ob/ob mice, increases length and tortuosity of microvessels (73), and synergistically with VEGF promotes angiogenesis (11,73). The increased length of the central feed arteriole is therefore not consistent with decreased leptin. Together this does not suggest a clear pattern, but does support that angiogenic factors are dysregulated in ob/ob mice.

Inflammatory nature of cytokines

Cytokines induce structural and functional alterations in endothelial cells and this is important both for angiogenesis and in the inflammatory response. There is a well documented association between diabetes, endothelial dysfunction, rarefaction and a pro-inflammatory state (41,56). Pro-inflammatory cytokines include: IL-1, IL-17, IFNgamma, KC, TNFalpha, RANTES, IL-2 (required for the full immune response, (61)), IL-4, IL-6 and

IL-12 (22,54,61,66,74). Evidence for a pro-inflammatory state in the db/db mice is suggested by elevated IL-1 and KC, and in the ob/ob by elevated IL-1, IFNgamma, KC, RANTES and IL-2. Anti-inflammatory cytokines include MIP-1b, IL-2, IL-4, IL-9, IL-10, IL-12 and IL-13 (29,46,61,74). Further evidence of inflammation in the db/db mice is suggested by decreased IL-2, IL-4, IL-9, IL-10, IL-12 and IL-13. Evidence of inflammation in the ob/ob mice is suggested by decreased IL-9 only, with IL-2 (also pro-inflammatory) and IL-13, instead, being markedly elevated. In general, the ob/ob mice show elevated pro-inflammatory cytokine levels, while the db/db mice show diminished anti-inflammatory cytokine levels; while both could be interpreted as pro-inflammatory states, the phenotypes mediating the pro-inflammatory state are quite different for these two models.

An important question is how the inflammatory process affects angiogenesis. The balance between inflammation and angiogenesis in endothelial cells is thought to be regulated by Angiopoietin-1 and Angiopoietin-2 (Ang-2). Ang-2, by interaction with TNFalpha results in inflammation while interaction with VEGF results in angiogenesis; further, Ang-1 is responsible for maintaining the resting state of the endothelium (28,38). The evidence suggests that over-expression of inflammatory cytokines could lead to the early expression of angiogenic factors. For example, IL-1beta and TNFalpha both induce VEGF (45). IL-1beta, TNFalpha, and GM-CSF stimulate neovascularization (6). A final consideration is the role of elevated pro-inflammatory cytokines in association with endothelial dysfunction. Little is published regarding endothelial dysfunction in the db/db mice, however there are several reports of endothelial dysfunction in ob/ob mice (53,77). Cytokines associated with protecting from endothelial dysfunction include: IL-1 (60), IL-4 (66), IL-6 (55) and IL-10 (21,80). Of these, IL-1alpha is elevated in both db/db and ob/ob, IL-4 IL-6 and IL-10 are suppressed in db/db, and IL-1beta is elevated in ob/ob and decreased in db/db. IL-17, which contributes to endothelial dysfunction (44) is increased in ob/ob compared to db/db. The present study shows evidence of a proinflammatory state for both the db/db and ob/ob mice, which may be both associated with endothelial dysfunction and contributory to rarefaction.

Conclusions

Our key data describes the architecture of the terminal arteriolar networks for db/db and ob/ob mice, showing structural remodeling that appears to reduce oxygen delivery capacity that is distinct in each, and associated with decreased pro-angiogenic cytokine levels in db/db. Functional rarefaction is likewise present within the networks for both db/db and ob/ob, and across networks for the ob/ob model based on variability of influx. Lastly, a pro-inflammatory state is supported for both the db/db and ob/ob mice, based on the plasma cytokine levels.

Acknowledgments

Thanks to Saumya Sharma for technical assistance.

Grants and support: NIH DK68401 AHA 0655908T

References

1. Alì G, Boldrini L, Lucchi M, Picchi A, Dell'Omodarme M, Prati MC, Mussi A, Corsi V, Fontanini G. Treatment with interleukin-2 in malignant pleural mesothelioma: immunological and angiogenetic assessment and prognostic impact. Br. J. Cancer. 2009; 101:1869–1875. [PubMed: 19935800]
2. Aplin AC, Fogel E, Nicosia RF. MCP-1 promotes mural cell recruitment during angiogenesis in the aortic ring model. Angiogenesis. 2010 June 23. 2010.

3. Baez S. An open cremaster muscle preparation for the study of blood vessels by in vivo microscopy. Microvascular Research. 1973; 5:384–394. [PubMed: 4709735]
4. Banks AS, Davis SM, Bates SH, Myers MG. Activation of downstream signals by the long form of the leptin receptor. J. Biol. Chem. 2000; 275:14563–14572. [PubMed: 10799542]
5. Barcelos LS, Coelho AM, Russo RC, Guabiraba R, Souza ALS, Bruno-Lima G, Proudfoot AEI, Andrade SP, Teixeira MM. Role of the chemokines CCL3/MIP-1 alpha and CCL5/RANTES in sponge-induced inflammatory angiogenesis in mice. Microvasc. Res. 2009; 78:148–154. [PubMed: 19427874]
6. BenEzra D, Griffin BW, Maftzir G, Aharonov O. Thrombospondin and in vivo angiogenesis induced by basic fibroblast growth factor or lipopolysaccharide. Invest. Ophthalmol. Vis. Sci. 1993; 34:3601–3608. [PubMed: 8258518]
7. Berg BR, Sarelius IH. Functional capillary organization in striated muscle. Am. J. Physiol. 1995; 268:H1215–H1222. [PubMed: 7900875]
8. Berne, R. Berne & Levy physiology. 6th ed.. Philadelphia PA: Mosby/Elsevier; 2010. 2010
9. Bohlen HG, Niggl BA. Adult microvascular disturbances as a result of juvenile onset diabetes in Db/Db mice. Blood Vessels. 1979; 16:269–276. [PubMed: 508951]
10. Burgess JK, Boustany S, Moir LM, Weckmann M, Lau JY, Grafton K, Baraket M, Hansbro PM, Hansbro NG, Foster PS, Black JL, Oliver BG. Reduction of tumstatin in asthmatic airways contributes to angiogenesis, inflammation, and hyperresponsiveness. Am. J. Respir. Crit. Care Med. 2010; 181:106–115. [PubMed: 19875687]
11. Cao R, Brakenhielm E, Wahlestedt C, Thyberg J, Cao Y. Leptin induces vascular permeability and synergistically stimulates angiogenesis with FGF-2 and VEGF. Proc. Natl. Acad. Sci. U.S.A. 2001; 98:6390–6395. [PubMed: 11344271]
12. Carmi Y, Voronov E, Dotan S, Lahat N, Rahat MA, Fogel M, Huszar M, White MR, Dinarello CA, Apte RN. The role of macrophage-derived IL-1 in induction and maintenance of angiogenesis. J. Immunol. 2009; 183:4705–4714. [PubMed: 19752225]
13. Chen J, Stinnett A. Ang-1 gene therapy inhibits hypoxia-inducible factor-1alpha (HIF-1alpha)-prolyl-4-hydroxylase-2, stabilizes HIF-1alpha expression, and normalizes immature vasculature in db/db mice. Diabetes. 2008; 57:3335–3343. [PubMed: 18835934]
14. Choi KM, Kashyap PC, Dutta N, Stoltz GJ, Ordog T, Shea Donohue T, Bauer AJ, Linden DR, Szurszewski JH, Gibbons SJ, Farrugia G. CD206-positive M2 macrophages that express heme oxygenase-1 protect against diabetic gastroparesis in mice. Gastroenterology. 2010; 138:2399–2409. 2409.e1. [PubMed: 20178793]
15. Cianfarani F, Tommasi R, Failla CM, Viviano MT, Annessi G, Papi M, Zambruno G, Odorisio T. Granulocyte/macrophage colony-stimulating factor treatment of human chronic ulcers promotes angiogenesis associated with de novo vascular endothelial growth factor transcription in the ulcer bed. Br. J. Dermatol. 2006; 154:34–41. [PubMed: 16403091]
16. Courtice FC. The blood volume of normal animals. J. Physiol. (Lond.). 1943; 102:290–305. [PubMed: 16991609]
17. Curfs JH, Meis JF, Hoogkamp-Korstanje JA. A primer on cytokines: sources, receptors, effects, and inducers. Clin. Microbiol. Rev. 1997; 10:742–780. [PubMed: 9336671]
18. Currie C, Morgan C, Peters J. The epidemiology and cost of inpatient care for peripheral vascular disease, infection, neuropathy, and ulceration in diabetes. Diabetes Care. 1998; 21:42–48. [PubMed: 9538969]
19. Davies M, Lund R, Mathew S, Hruska K. Low Turnover Osteodystrophy and Vascular Calcification Are Amenable to Skeletal Anabolism in an Animal Model of Chronic Kidney Disease and the Metabolic Syndrome. J Am Soc Nephrol. 2005; 16:917–928. [PubMed: 15743994]
20. Dentelli P, Del Sorbo L, Rosso A, Molinar A, Garbarino G, Camussi G, Pegoraro L, Brizzi MF. Human IL-3 stimulates endothelial cell motility and promotes in vivo new vessel formation. J. Immunol. 1999; 163:2151–2159. [PubMed: 10438956]
21. Didion SP, Kinzenbaw DA, Schrader LI, Chu Y, Faraci FM. Endogenous interleukin-10 inhibits angiotensin II-induced vascular dysfunction. Hypertension. 2009; 54:619–624. [PubMed: 19620507]

22. Doupis J, Lyons TE, Wu S, Gnardellis C, Dinh T, Veves A. Microvascular reactivity and inflammatory cytokines in painful and painless peripheral diabetic neuropathy. J. Clin. Endocrinol. Metab. 2009; 94:2157–2163. [PubMed: 19276232]

23. Dube MG, Torto R, Kalra SP. Increased leptin expression selectively in the hypothalamus suppresses inflammatory markers CRP and IL-6 in leptin-deficient diabetic obese mice. Peptides. 2008; 29:593–598. [PubMed: 18325632]

24. Emanueli C, Salis M, Pinna A, Stacca T, Milia A, Spano A, Chao J, Chao L, Sciola L, Madeddu P. Prevention of Diabetes-Induced Microangiopathy by Human Tissue Kallikrein Gene Transfer. Circulation. 2002; 106:993–999. [PubMed: 12186806]

25. Emanueli C, Caporali A, Krankel N, Cristofaro B, Van Linthout S, Madeddu P. Type-2 diabetic Lepr(db/db) mice show a defective microvascular phenotype under basal conditions and an impaired response to angiogenesis gene therapy in the setting of limb ischemia. Front. Biosci. 2007; 12:2003–2012. [PubMed: 17127438]

26. Entabi F, Albadawi H, Stone DH, Sroufe R, Conrad MF, Watkins MT. Hind limb ischemia-reperfusion in the leptin receptor deficient (db/db) mouse. J. Surg. Res. 2007; 139:97–105. [PubMed: 17292407]

27. Fang Y, Shen J, Yao M, Beagley K, Hambly B, Bao S. Granulocyte-macrophage colony-stimulating factor enhances wound healing in diabetes via upregulation of proinflammatory cytokines. British Journal of Dermatology. 2010; 162:478–486. [PubMed: 19799605]

28. Fiedler U, Reiss Y, Scharpfenecker M, Grunow V, Koidl S, Thurston G, Gale NW, Witzenrath M, Rosseau S, Suttorp N, Sobke A, Herrmann M, Preissner KT, Vajkoczy P, Augustin HG. Angiopoietin-2 sensitizes endothelial cells to TNF-alpha and has a crucial role in the induction of inflammation. Nat. Med. 2006; 12:235–239. [PubMed: 16462802]

29. Fisman EZ, Adler Y, Tenenbaum A. Biomarkers in cardiovascular diabetology: interleukins and matrixins. Adv Cardiol. 2008; 45:44–64. [PubMed: 18230955]

30. Fox RJ, Frame MD. Arteriolar flow recruitment with vitronectin receptor stimulation linked to remote wall shear stress. Microvasc. Res. 2002; 64:414–424. [PubMed: 12453436]

31. Gómez-Ambrosi J, Catalán V, Rodríguez A, Ramírez B, Silva C, Gil MJ, Salvador J, Frühbeck G. Involvement of serum vascular endothelial growth factor family members in the development of obesity in mice and humans. J Nutr Biochem. 2010; 21:774–780. [PubMed: 19615882]

32. Goodwill AG, Frisbee SJ, Stapleton PA, James ME, Frisbee JC. Impact of chronic anticholesterol therapy on development of microvascular rarefaction in the metabolic syndrome. Microcirculation. 2009; 16:667–684. [PubMed: 19905967]

33. Gove ME, Rhodes DH, Pini M, van Baal JW, Sennello JA, Fayad R, Cabay RJ, Myers MG, Fantuzzi G. Role of leptin receptor-induced STAT3 signaling in modulation of intestinal and hepatic inflammation in mice. J. Leukoc. Biol. 2009; 85:491–496. [PubMed: 19052144]

34. Hill MA, Simpson BE, Meininger GA. Altered cremaster muscle hemodynamics due to disruption of the deferential feed vessels. Microvasc. Res. 1990; 39:349–363. [PubMed: 2362557]

35. Hofmann S, Dong H, Li Z, Cai W, Altomonte J, Thung S, Zeng F, Fisher E, Vlassara H. Improved Insulin Sensitivity Is Associated With Restricted Intake of Dietary Glycoxidation Products in the db/db Mouse. Diabetes. 2002; 51:2082–2089. [PubMed: 12086936]

36. Igel M, Becker W, Herberg L, Joost HG. Hyperleptinemia, leptin resistance, and polymorphic leptin receptor in the New Zealand obese mouse. Endocrinology. 1997; 138:4234–4239. [PubMed: 9322935]

37. Ikeda U, Ikeda M, Oohara T, Oguchi A, Kamitani T, Tsuruya Y, Kano S. Interleukin 6 stimulates growth of vascular smooth muscle cells in a PDGF-dependent manner. Am. J. Physiol. 1991; 260:H1713–H1717. [PubMed: 1709793]

38. Imhof BA, Aurrand-Lions M. Angiogenesis and inflammation face off. Nat. Med. 2006; 12:171–172. [PubMed: 16462798]

39. Kamiya A, Ando J, Shibata M, Wakayama H. The efficiency of the vascular-tissue system for oxygen transport in the skeletal muscles. Microvasc. Res. 1990; 39:169–185. [PubMed: 2352488]

40. Kim G, Lee J, Ryu H, Wei J, Seong C, Kim J. Proinflammatory cytokine IL-1beta stimulates IL-8 synthesis in mast cells via a leukotriene B4 receptor 2-linked pathway, contributing to angiogenesis. J. Immunol. 2010; 184:3946–3954. [PubMed: 20194723]

41. Ko S, Cao W, Liu Z. Hypertension management and microvascular insulin resistance in diabetes. Curr. Hypertens. Rep. 2010; 12:243–251. [PubMed: 20582734]
42. Kyzer S, Binyamini J, Chaimoff C, Fishman P. The effect of surgically induced weight reduction on the serum levels of the cytokines: interleukin-3 and tumor necrosis factor. Obes Surg. 1999; 9:229–234. [PubMed: 10484307]
43. Lin C, Shyu K, Wang B, Chang H, Chen Y, Chiu J. Chrysin suppresses IL-6-induced angiogenesis via down-regulation of JAK1/STAT3 and VEGF: an in vitro and in ovo approach. J. Agric. Food Chem. 2010; 58:7082–7087. [PubMed: 20443595]
44. Madhur MS, Lob HE, McCann LA, Iwakura Y, Blinder Y, Guzik TJ, Harrison DG. Interleukin 17 promotes angiotensin II-induced hypertension and vascular dysfunction. Hypertension. 2010; 55:500–507. [PubMed: 20038749]
45. Margetts PJ, Kolb M, Yu L, Hoff CM, Holmes CJ, Anthony DC, Gauldie J. Inflammatory cytokines, angiogenesis, and fibrosis in the rat peritoneum. Am. J. Pathol. 2002; 160:2285–2294. [PubMed: 12057931]
46. Meagher C, Arreaza G, Peters A, Strathdee CA, Gilbert PA, Mi Q, Santamaria P, Dekaban GA, Delovitch TL. CCL4 protects from type 1 diabetes by altering islet beta-cell-targeted inflammatory responses. Diabetes. 2007; 56:809–817. [PubMed: 17327452]
47. Mentor-Marcel RA, Bobe G, Barrett KG, Young MR, Albert PS, Bennink MR, Lanza E, Colburn NH. Inflammation-associated serum and colon markers as indicators of dietary attenuation of colon carcinogenesis in ob/ob mice. Cancer Prev Res (Phila Pa). 2009; 2:60–69.
48. Milkiewicz M, Brown MD, Egginton S, Hudlicka O. Association between shear stress, angiogenesis, and VEGF in skeletal muscles in vivo. Microcirculation. 2001; 8:229–241. [PubMed: 11528531]
49. Mishima Y, Kuyama A, Tada A, Takahashi K, Ishioka T, Kibata M. Relationship between serum tumor necrosis factor-alpha and insulin resistance in obese men with Type 2 diabetes mellitus. Diabetes Res. Clin. Pract. 2001; 52:119–123. [PubMed: 11311966]
50. Mustafa SS, Rivers RJ, Frame MD. Microcirculatory basis for nonuniform flow delivery with intravenous nitroprusside. Anesthesiology. 1999; 91:723–731. [PubMed: 10485784]
51. Nishigaki K, Faber JE, Ohyanagi M. Occlusion of cremaster collateral circulation alters microvascular reactivity. Microvasc. Res. 1991; 41:173–183. [PubMed: 1646943]
52. Oakes N, Thalen P, Aasum E, Edgley A, Larsen T, Furler S, Ljung B, Severson D. Cardiac metabolism in mice: tracer method developments and in vivo application revealing profound metabolic inflexibility in diabetes. Am J Physiol Endocrinol Metab. 2006; 290:E870–E881. [PubMed: 16352676]
53. Okon EB, Szado T, Laher I, McManus B, van Breemen C. Augmented contractile response of vascular smooth muscle in a diabetic mouse model. J. Vasc. Res. 2003; 40:520–530. [PubMed: 14646372]
54. Park SJ, Lee YC. Interleukin-17 regulation: an attractive therapeutic approach for asthma. Respir. Res. 2010; 11:78. [PubMed: 20565710]
55. Park Y, Capobianco S, Gao X, Falck JR, Dellsperger KC, Zhang C. Role of EDHF in type 2 diabetes-induced endothelial dysfunction. AJP: Heart and Circulatory Physiology. 2008; 295:H1982–H1988. [PubMed: 18790831]
56. Pasarica M, Sereda OR, Redman LM, Albarado DC, Hymel DT, Roan LE, Rood JC, Burk DH, Smith SR. Reduced adipose tissue oxygenation in human obesity: evidence for rarefaction, macrophage chemotaxis, and inflammation without an angiogenic response. Diabetes. 2009; 58:718–725. [PubMed: 19074987]
57. Pickens SR, Volin MV, Mandelin AM, Kolls JK, Pope RM, Shahrara S. IL-17 contributes to angiogenesis in rheumatoid arthritis. J. Immunol. 2010; 184:3233–3241. [PubMed: 20173024]
58. Pini M, Fantuzzi G. Enhanced production of IL-17A during zymosan-induced peritonitis in obese mice. J. Leukoc. Biol. 2010; 87:51–58. [PubMed: 19745158]
59. Priestman D, Spoel A, Butters T, Dwek R, Platt F. N-butyldeoxynojirimycin causes weight loss as a result of appetite suppression in lean and obese mice. Diabetes, Obesity and Metabolism. 2008; 10:159–166.

60. Qian L, Wang H, Qiu W, Huang H, Bruce IC, Xia Q. Interleukin-2 protects against endothelial dysfunction induced by high glucose levels in rats. Vascul. Pharmacol. 2006; 45:374–382. [PubMed: 16837248]
61. Remick, D. Cytokines in health and disease. 2nd ed.. New York: M. Dekker; 1997. 1997
62. Rumore-Maton B, Elf J, Belkin N, Stutevoss B, Seydel F, Garrigan E, Litherland SA. M-CSF and GM-CSF regulation of STAT5 activation and DNA binding in myeloid cell differentiation is disrupted in nonobese diabetic mice. Clin. Dev. Immunol. 2008; 2008:769795. [PubMed: 19165346]
63. Sarelius I, Duling B. Direct measurement of microvessel hematocrit, red cell flux, velocity, and transit time. Am J Physiol Heart Circ Physiol. 1982; 243:H1018–H1026.
64. Simpson PB, Mistry MS, Maki RA, Yang W, Schwarz DA, Johnson EB, Lio FM, Alleva DG. Cuttine edge: diabetes-associated quantitative trait locus, Idd4, is responsible for the IL-12p40 overexpression defect in nonobese diabetic (NOD) mice. J. Immunol. 2003; 171:3333–3337. [PubMed: 14500624]
65. Sokal, R. Biometry : the principles and practice of statistics in biological research. 3rd ed.. New York: W.H. Freeman; 1995. 1995
66. Soltesz P, Der H, Veres K, Laczik R, Sipka S, Szegedi G, Szodoray P. Immunological features of primary anti-phospholipid syndrome in connection with endothelial dysfunction. Rheumatology (Oxford). 2008; 47:1628–1634. [PubMed: 18782854]
67. Spranger J, Kroke A, Möhlig M, Hoffmann K, Bergmann MM, Ristow M, Boeing H, Pfeiffer AFH. Inflammatory cytokines and the risk to develop type 2 diabetes: results of the prospective population-based European Prospective Investigation into Cancer and Nutrition (EPIC)-Potsdam Study. Diabetes. 2003; 52:812–817. [PubMed: 12606524]
68. Srinivasan S, Bolick DT, Hatley ME, Natarajan R, Reilly KB, Yeh M, Chrestensen C, Sturgill TW, Hedrick CC. Glucose regulates interleukin-8 production in aortic endothelial cells through activation of the p38 mitogen-activated protein kinase pathway in diabetes. J. Biol. Chem. 2004; 279:31930–31936. [PubMed: 15145956]
69. Stapleton PA, Goodwill AG, James ME, D'Audiffret AC, Frisbee JC. Differential impact of familial hypercholesterolemia and combined hyperlipidemia on vascular wall and network remodeling in mice. Microcirculation. 2010; 17:47–58. [PubMed: 20141600]
70. Surmi BK, Webb CD, Ristau AC, Hasty AH. Absence of Macrophage Inflammatory Protein-1{alpha} Does Not Impact Macrophage Accumulation in Adipose Tissue of Diet Induced Obese Mice. Am J Physiol Endocrinol Metab. 2010 June 15. 2010.
71. Sweeney TE, Sarelius IH. Spatial heterogeneity in striated muscle arteriolar tone, cell flow, and capillarity. Am. J. Physiol. 1990; 259:H124–H136. [PubMed: 2375398]
72. Sweeney T, Sarelius I. Arteriolar control of capillary cell flow in striated muscle. Circ Res. 1989; 64:112–120. [PubMed: 2909294]
73. Talavera-Adame D, Xiong Y, Zhao T, Arias AE, Sierra-Honigmann MR, Farkas DL. Quantitative and morphometric evaluation of the angiogenic effects of leptin. J Biomed Opt. 2008; 13:064017. [PubMed: 19123663]
74. Tedgui A, Mallat Z. Cytokines in atherosclerosis: pathogenic and regulatory pathways. Physiol. Rev. 2006; 86:515–581. [PubMed: 16601268]
75. Tran ED, Schmid-Schönbein GW. An in-vivo analysis of capillary stasis and endothelial apoptosis in a model of hypertension. Microcirculation. 2007; 14:793–804. [PubMed: 17924279]
76. Tuttle HA, Davis-Gorman G, Goldman S, Copeland JG, McDonagh PF. Proinflammatory cytokines are increased in type 2 diabetic women with cardiovascular disease. J. Diabetes Complicat. 2004; 18:343–351. [PubMed: 15531184]
77. Winters B, Mo Z, Brooks-Asplund E, Kim S, Shoukas A, Li D, Nyhan D, Berkowitz DE. Reduction of obesity, as induced by leptin, reverses endothelial dysfunction in obese (Lep(ob)) mice. J. Appl. Physiol. 2000; 89:2382–2390. [PubMed: 11090593]
78. Wolf U, Wolf M, Choi J, Levi M, Choudhury D, Hull S, Coussirat D, Paunescu L, Safonova L, Michalos A, Mantulin W, Gratton E. Localized irregularities in hemoglobin flow and oxygenation in calf muscle in patients with peripheral vascular disease detected with near-infrared spectrophotometry. J. Vasc. Surg. 2003; 37:1017. [PubMed: 12756348]

79. Yamaji-Kegan K, Su Q, Angelini DJ, Johns RA. IL-4 is proangiogenic in the lung under hypoxic conditions. J. Immunol. 2009; 182:5469–5476. [PubMed: 19380795]

80. Zemse SM, Hilgers RHP, Webb RC. Interleukin-10 counteracts impaired endothelium-dependent relaxation induced by ANG II in murine aortic rings. Am. J. Physiol. Heart Circ. Physiol. 2007; 292:H3103–H3108. [PubMed: 17322422]

81. Zinman B, Hanley AJ, Harris SB, Kwan J, Fantus IG. Circulating tumor necrosis factor-alpha concentrations in a native Canadian population with high rates of type 2 diabetes mellitus. J. Clin. Endocrinol. Metab. 1999; 84:272–278. [PubMed: 9920095]

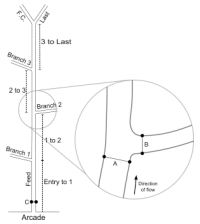

Figure 1.

Schematic of network showing locations of architectural measurements. Branches are numbered consecutively as they arise along the central feed. At the last bifurcation the anatomically smaller diameter vessel is designated as the last branch, and the larger diameter vessel is designated the feed continuation (F.C.). Inter-branch lengths (indicated by dotted lines) are measured from the center of the previous bifurcation to the current bifurcation; the total length is the sum of these values. Feed diameters are measured for each bifurcation one feed tube diameter upstream (A) of the branch wall. Branch diameters are measured for each branch one tube diameter downstream from the feed wall (B). Red blood cell influx to the network is measured at the entrance to the network (C), and then at sequential branches.

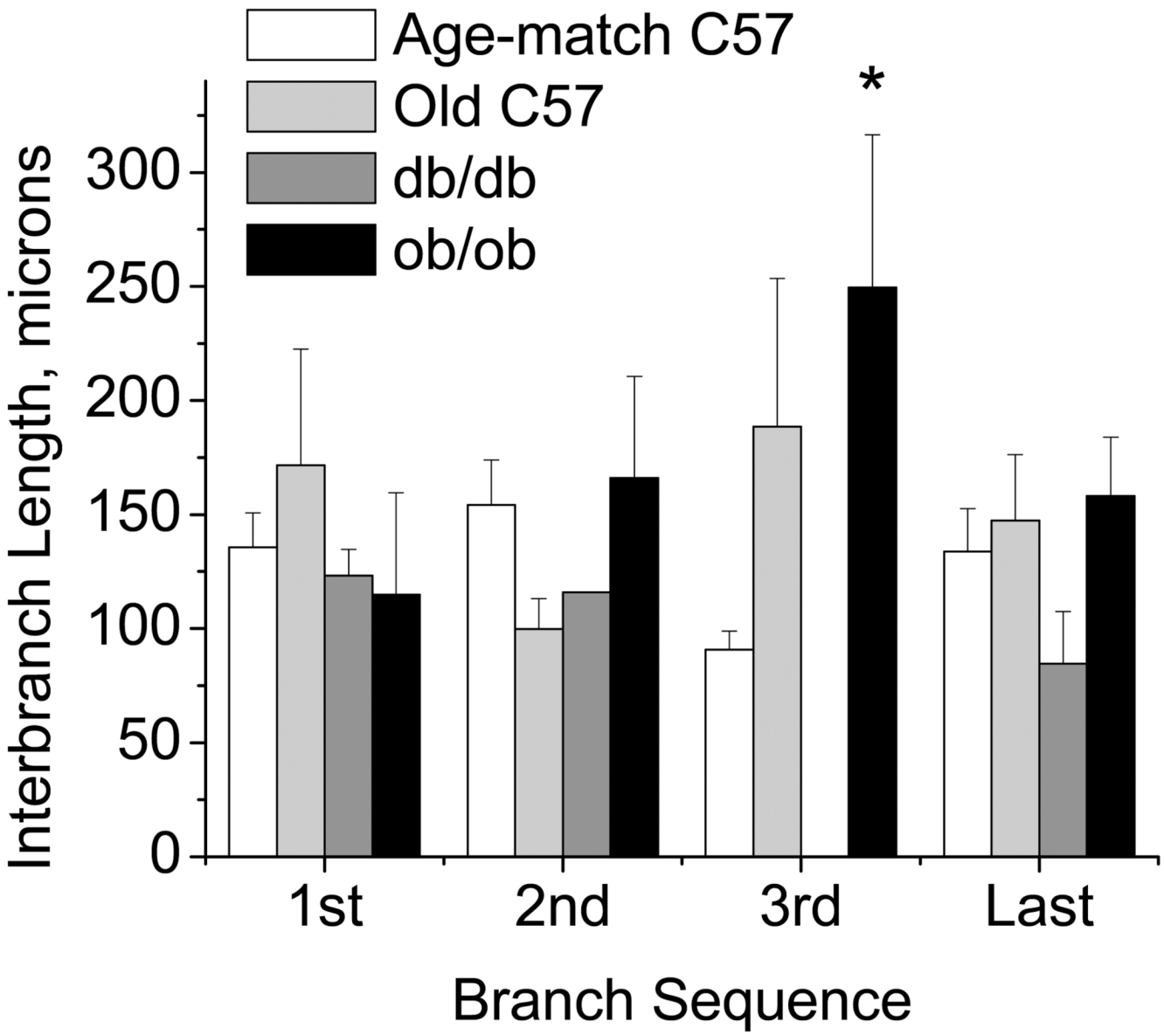

Figure 2.

Interbranch lengths for each strain (mean±SE: Age-match C57/bl6 n=29, Old C57/bl6 n = 5; db/db n = 5; ob/ob n = 6). Distances from the entrance of the network to the first branch (1st), first to second (2nd), second to third (3rd), and third to last (last) are shown. Branch 2 occurred in only a single db/db, and branch 3 occurred in no db/db mice. Most interbranch distances did not differ by strain, however variability was different by strain (see text). *ob/ob greater than age-matched C57, $P<0.05$.

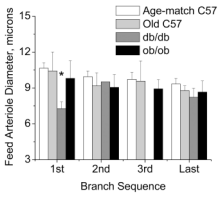

Figure 3.

Diameter of the feed segments measured one tube diameter upstream of the bifurcation (1,2,3,last) for each strain (mean±SE: Age-match C57/bl6 n=29, Old C57/bl6 n = 5; db/db n = 5; ob/ob n = 6). *db/db less than age matched C57, $P<0.05$.

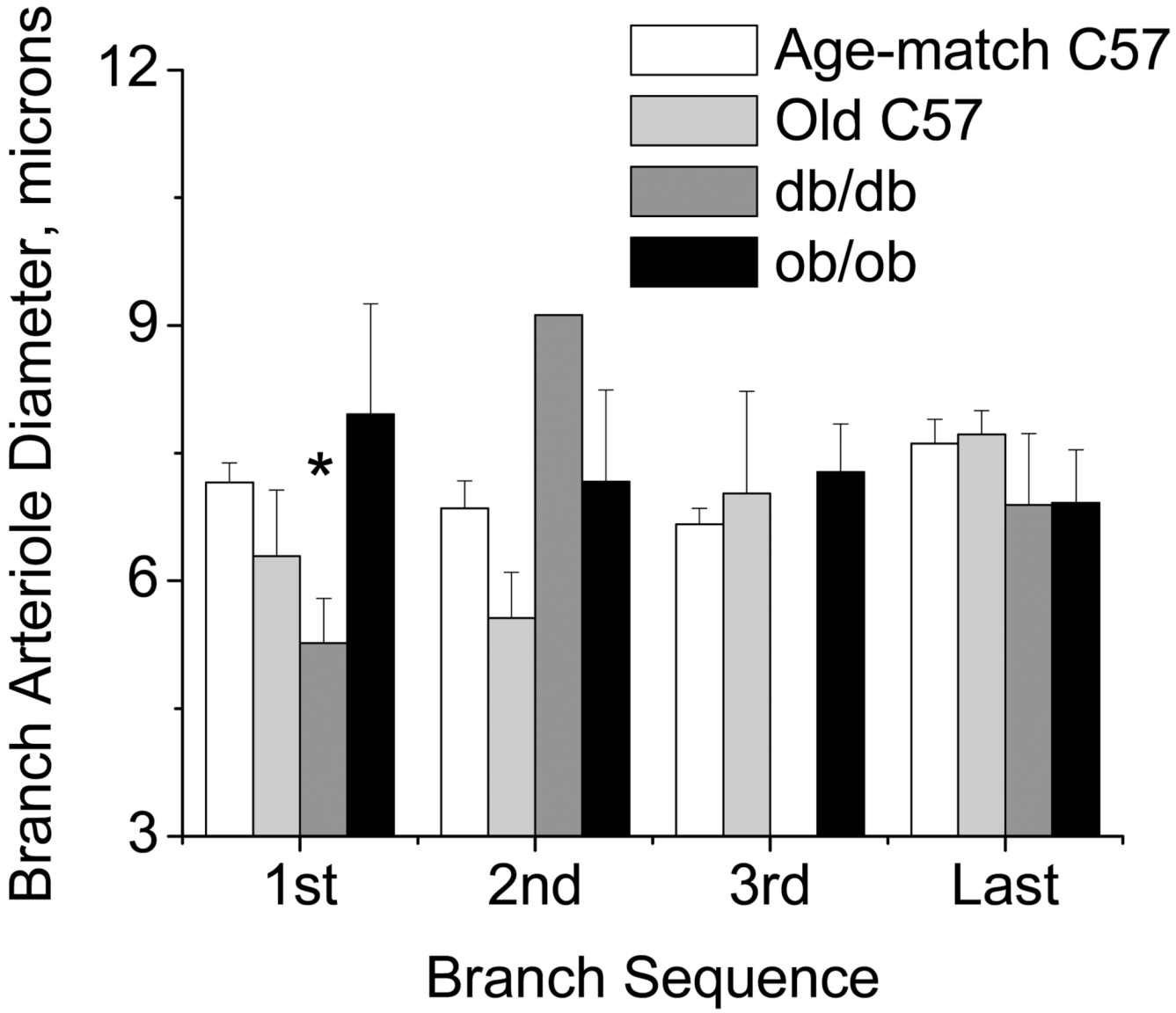

Figure 4.
Diameter of the branch segments measured one tube diameter downstream of the bifurcation (1,2,3,last) for each strain (mean±SE: Age-match C57/bl6 n=29, Old C57/bl6 n = 5; db/db n = 5; ob/ob n = 6). *db/db less than age matched C57, P<0.05.

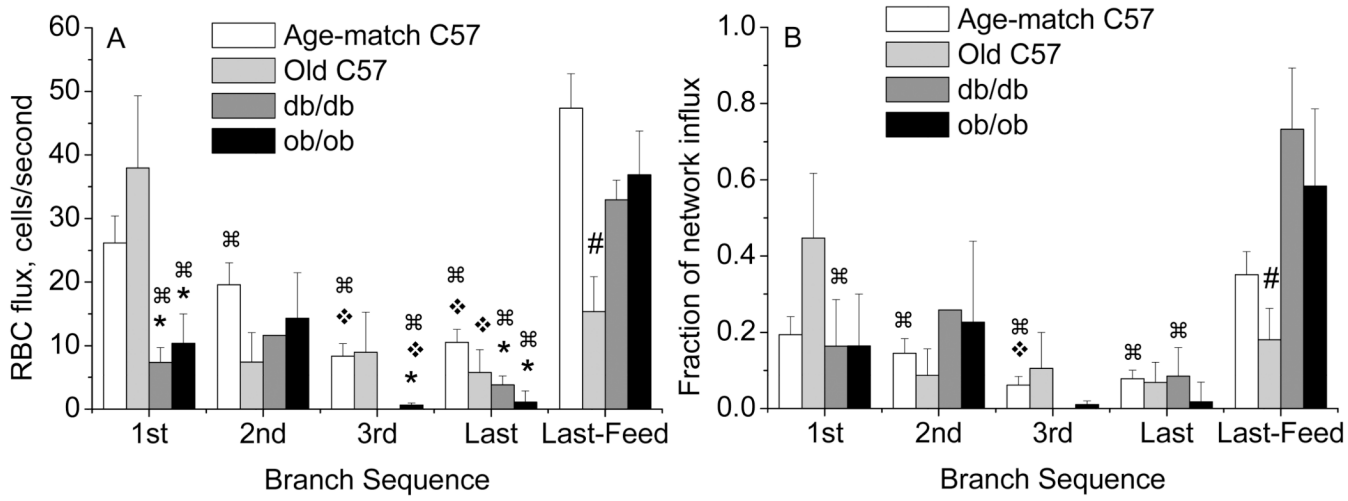

Figure 5.

Red blood cell (RBC) flux distribution to sequential branches (1,2,3,last) of the network for each strain (mean±SE: Age-match C57/bl6 n=29, Old C57/bl6 n = 5; db/db n = 5; ob/ob n = 6). (A) RBC flux shown as cells/second; (B) RBC flux shown as the fraction of the total network influx. *differs from Age-matched or Old C57 at that branch, #Old C57 less than others at Last-Feed (panel A) or less than db/db (panel B); ❖ differs from 1st branch within that group; ⌘ differs from Last-Feed within that group, $P<0.05$.

Table 1

Demographics of populations of mice used for architecture and flux vs. plasma cytokine data.

					Blood Glucose (mg/dl)		Systemic Hematocrit (%)	
	N	Average Age	Min/Max (days)	Weight (g)	Post induction	Post protocol	Post induction	Post protocol
Population for architecture and flux data[a]								
C57/bl6-Age-matched	29	95±2[e]	76/118	27.0±0.4[e]	139.4±4.3[b]	56.5±5.3[f]	51±1.0	46±0.9[f]
C57/bl6-Old	5	140±3.5[c]	132/152	29.8±0.5[c]	134.5±7.3[b]	40.6±7[f]	48±1.9	45±0.8
db/db	5	91±3.5[e]	79/99	48.3±1.8[c,e]	434.2±78[c,e]	389.2±32[c,e]	49±1.9	54±2.1[c,e]
ob/ob	6	82±2.9[e]	74/91	48.2±1.8[c,e]	242.8±30[c,d,e]	430.0±39[c,e,f]	52±0.5	53±1.9
Population for plasma cytokine data[a]								
C57/bl6-Age-matched	10	90.2±3.2[e]	75/97	26.4±0.8[e]	151.7±4.8[b]	88.5±11.8[b,f]	52±0.4	48±1.3[f]
C57/bl6-Old	6	157±17[c]	124/214	33.0±2.5[c]	126.7±5[b,c]	70.3±7.6[b,f]	52±1.7	47±0.8
db/db	12	81.7±3.5[e]	62/98	44.9±2.4[c,e]	373.3±47[c,e]	477.0±49[c,e]	50±2.6	48±2.0
ob/ob	12	75.0±3.7[e]	57/97	47.8±1.6[c,e]	280.5±27[c,e]	429.1±35[c,e,f]	51±2.6	49±1.3

Entries are mean±SEM.

[a] Mice in both groups: C57/bl6 n=0; db/db n=2; ob/ob n=2.

[b] Within normal blood glucose range for mice.

[c] p<0.05 vs. C57/bl6 Age-matched.

[d] p<0.05 db/db vs. ob/ob.

[e] p<0.05 vs. Old C57/bl6.

[f] p<0.05 post induction vs. post protocol

Table 2

Network Lengths and Number of Branches

Strain	N	Number of Branches	Total Network Length (μm)
C57/bl6-Age-matched	29	3.4 ± 0.12	454 ± 33
C57/bl6-Old	5	4 ± 0.32	637 ± 76
db/db	5	2.0 ± 0.30*	222 ± 25*
ob/ob	6	4.1 ± 0.30	728 ± 179

Entries are mean ± SEM;

* differs from others, $p<0.05$

Table 3

Ratio of Coefficient of Variation* compared to age-matched C57/bl6

	interbranch lengths				
	entry to 1st	1st to 2nd	2nd to 3rd	3rd to last	
db/db:age-matched C57/bl6	0.35			0.80	
ob/ob:age-matched C57/bl6	1.61	0.96	1.35	0.53	
old:age-matched C57/bl6	1.12	0.44	1.59	0.58	
	feed diameter				
	1st	2nd	3rd	last	
db/db:age-matched C57/bl6	0.75			0.78	
ob/ob:age-matched C57/bl6	1.56	1.12	0.64	1.00	
old:age-matched C57/bl6	1.44	1.03	1.19	0.39	
	branch diameter				
	1st	2nd	3rd	last	
db/db:age-matched C57/bl6	1.27			1.34	
ob/ob:age-matched C57/bl6	2.29	1.44	1.25	1.09	
old:age-matched C57/bl6	1.58	0.85	2.50	0.40	
	flux as fraction of inflow				
	1st	2nd	3rd	last	last Feed
db/db:age-matched C57/bl6	1.27			1.24	0.53
ob/ob:age-matched C57/bl6	1.55	1.60	1.27	4.51	0.92
old:age-matched C57/bl6	0.65	1.23	1.04	1.09	1.10
	flux cells/s				
	1st	2nd	3rd	last	last Feed
db/db:age-matched C57/bl6	0.55			0.69	0.57
ob/ob:age-matched C57/bl6	1.09	2.08	0.17	0.85	1.27
old:age-matched C57/bl6	2.68	1.34	3.19	1.72	1.02

* entries are the ratio of the coefficient of variation, CV = sd/mean, for the test groups divided by the CV for the age-matched C57/bl6.

Table 4

Plasma Cytokine levels

cytokine	C57/bl6 (Age-matched)[a]	C57/bl6 (Old)	db/db	ob/ob
IL-1alpha	21.3± 4.7	35.7± 4.0	50.2± 3.6 *b,d*	65.8± 18.9 *b,d*
IL-1beta	169.5± 23.1	143.5± 17.9	61.4± 14 *b,d*	288.6± 90.6 *b,d*
IL-2	27.7± 4.4	28.2± 2.4	7.3± 1.2 *b,d*	182.8± 117.5 *b*
IL-3	5.9± 0.7	7.5± 1.2	1.7± 0.2 *b,d*	3.5± 0.6 *b,d*
IL-4	3.4± 0.4	5.4± 0.7	1.2± 0.1 *b,d*	4.9± 1.6 *c*
IL-5	18.4± 6.1	21.7± 4.6	6.0± 1.2 *b*	53.4± 30.6 *c*
IL-6	13.3± 2.7	8.5± 1.4	7.1± 0.9	21.0± 5.2 *c,d*
IL-9	31.4± 4.2	133± 38 *b*	4.6± 2.5 *b,d*	6.8± 1.5 *b,d*
IL-10	37.4± 5.4	64.3± 12.7	9.8± 3.8 *b,d*	42.4± 16.6 *c*
IL-12(p40)	64.7± 9.5	54.5± 15.6	14.1± 3.6 *b,d*	37.1± 12.9 *c*
IL-12(p70)	35.2± 10.0	31.9± 8.5	7.9± 2.6 *b,d*	60.1± 28.8 *c*
IL-13	14.5± 2.3	40.9± 7.7 *b*	4.5± 1.5 *b,d*	122.5± 67.7 *b,c*
IL-17	51.6± 20.7	16.5± 2.4	9.5± 1.5 *d*	29.3± 10.3 *c*
GM-CSF	38.8± 3.6	46.1± 6.5	11.5± 1.9 *b,d*	20.9± 4.7 *b,c,d*
IFNgamma	22.9± 2.7	31.0± 4.8	9.0± 1.5 *b,d*	17.8± 4.5 *c*
KC[e]	29.2± 7.0	47.4± 8.8	134.9± 68.5 *b*	303.7± 171.5 *b,d*
TNFalpha	15.6± 3.5	12.8± 2.7	10.2± 2.1	13.7± 2.6
MCP-1	124.5± 15.3	187.9± 29.2	115.7± 27.3	133.5± 21.3
MIP-1beta	253.9± 37.9	299.6± 51.9	157.0± 28.2	1302± 979.2
RANTES	28.2± 5.7	45.3± 6.3	55.8± 9.9	141.5± 20 *b,c,d*
VEGF	10.3± 1.1	12.6± 1.5	3.0± 0.3 *b,d*	19.9± 4.1 *b,c*

Entries are mean±SEM, in pg/ml plasma. N=6 C57/bl6 (Old), N=10 C57/bl6 (Age-matched), N=12 db/db, N=12 ob/ob animals; serum was pooled in same-strain groups of 2–4 animals per analysis.

a age matched to db/db and ob/ob.

b p<0.05 vs. C57/bl6 95d

c p<0.05 db/db vs. ob/ob

d p<0.05 C57/bl6 140d

e KC is the murine ortholog of IL-8